doi:10.1093/brain/aww243 BRAIN 2016: 139; 3253–3266 | 3253

BRAIN
A JOURNAL OF NEUROLOGY

Whole-brain analysis reveals increased neuroanatomical asymmetries in dementia for hippocampus and amygdala

Christian Wachinger,[1,2,3] David H. Salat,[1,4] Michael Weiner[5] and Martin Reuter[1,3,4] for the Alzheimer's Disease Neuroimaging Initiative

Structural magnetic resonance imaging data are frequently analysed to reveal morphological changes of the human brain in dementia. Most contemporary imaging biomarkers are scalar values, such as the volume of a structure, and may miss the localized morphological variation of early presymptomatic disease progression. Neuroanatomical shape descriptors, however, can represent complex geometric information of individual anatomical regions and may demonstrate increased sensitivity in association studies. Yet, they remain largely unexplored. In this article, we introduce a novel technique to study shape asymmetries of neuroanatomical structures across subcortical and cortical brain regions. We demonstrate that neurodegeneration of subcortical structures in Alzheimer's disease is not symmetric. The hippocampus shows a significant increase in asymmetry longitudinally and both hippocampus and amygdala show a significantly higher asymmetry cross-sectionally concurrent with disease severity above and beyond an ageing effect. Our results further suggest that the asymmetry in these structures is undirectional and that primarily the anterior hippocampus becomes asymmetric. Based on longitudinal asymmetry measures we subsequently study the progression from mild cognitive impairment to dementia, demonstrating that shape asymmetry in hippocampus, amygdala, caudate and cortex is predictive of disease onset. The same analyses on scalar volume measurements did not produce any significant results, indicating that shape asymmetries, potentially induced by morphometric changes in subnuclei, rather than size asymmetries are associated with disease progression and can yield a powerful imaging biomarker for the early presymptomatic classification and prediction of Alzheimer's disease. Because literature has focused on contralateral volume differences, subcortical disease lateralization may have been overlooked thus far.

1 A.A. Martinos Center for Biomedical Imaging, Massachusetts General Hospital, Charlestown, MA 02129, USA
2 Department of Child and Adolescent Psychiatry, Psychosomatic and Psychotherapy, Ludwig-Maximilian-University, Munich, Germany
3 Computer Science and Artificial Intelligence Lab, Massachusetts Institute of Technology, Cambridge, MA, USA
4 Department of Radiology, Harvard Medical School, Boston MA, USA
5 University of California, San Francisco, San Francisco VA Medical Center, San Francisco CA, 94121 USA

Correspondence to: Christian Wachinger,
Waltherstr. 23, 80337 Munich,
Germany
E-mail: wachinger@gmail.com

Correspondence may also be addressed to: Martin Reuter,
149 Thirteenth Street, Suite 2301, Charlestown, MA 02129,
USA
E-mail: mreuter@nmr.mgh.harvard.edu

Keywords: brain asymmetry; Alzheimer's disease; longitudinal shape analysis; mixed effects models; survival analysis

Abbreviation: MCI = mild cognitive impairment

Received April 11, 2016. Revised August 5, 2016. Accepted August 12, 2016. Advance Access publication October 10, 2016

Introduction

Alzheimer's disease is the most common form of dementia with incidence rates further increasing in the future due to increasing life expectancy. Currently approved treatments for Alzheimer's disease relieve symptoms but do not target the underlying causes of the disease. It is expected that new treatment options will become available in the future that directly interfere with disease pathways (e.g. the amyloid cascade). Such treatment, however, requires the early identification of individuals with an elevated risk for developing dementia. Mild cognitive impairment (MCI) is associated with isolated memory loss, a common precursor to dementia in Alzheimer's disease. The neuropathological substrates of MCI are heterogeneous (Schneider *et al.*, 2009) and, despite the high rate of progression to Alzheimer's disease, a significant number of patients with MCI remain stable (Petersen *et al.*, 2009). A more accurate prediction of the likelihood for progression and the early detection of the disease requires a better understanding of disease trajectories. Longitudinal neuroimaging provides unique opportunities for studying trajectories because the measured atrophy correlates with neuron loss; imaging can therefore indicate the onset of the impairment in close temporal proximity (Jack *et al.*, 2013).

A key aspect for studying dementia trajectories is to map the spatial atrophy pattern across time. Early on, ^{18}F-fluorodeoxyglucose PET indicated significant right/left and frontal/parietal metabolic asymmetries in mild Alzheimer's disease (Grady *et al.*, 1988; Haxby *et al.*, 1990). This *in vivo* pattern of hypometabolism is found in the vast majority of clinically diagnosed Alzheimer's disease patients and in over 85% of pathologically confirmed Alzheimer's disease cases (Silverman *et al.*, 2001). Furthermore, as Alzheimer's disease progresses, right/left asymmetries are directionally stable and become more pronounced with time (Haxby *et al.*, 1990). Recent PET studies with ^{11}C-Pittsburgh compound B showed an asymmetric spatial distribution of amyloid-β and the positive correlation between asymmetries in amyloid-β deposition and hypometabolism (Frings *et al.*, 2015). Interestingly, disease severity was neither related to asymmetries of amyloid-β load nor to hypometabolism, suggesting that lateralization of pathology and neurodegeneration is not confined to disease onset, but a core feature throughout disease stages. The asymmetry in Alzheimer's disease was further confirmed in histopathological data (Stefanits *et al.*, 2012). On MRI, it was demonstrated that cortical atrophy occurred earlier and progressed faster in the left hemisphere than in the right in Alzheimer's disease patients (Thompson *et al.*, 2007; Long *et al.*, 2013). For subcortical structures the effect of the progression of Alzheimer's disease on anatomical asymmetry has only been investigated for the hippocampus and is less clear. Fox *et al.* (1996) reported an asymmetrical atrophy of the hippocampus that developed for patients with Alzheimer's disease, whereas more recent studies reported a decrease or sign flip in volume asymmetry for patients with dementia (Barnes *et al.*, 2005; Shi *et al.*, 2009).

We believe that stronger anatomical asymmetries have so far not been detected in MRI because volume measurements have been used, which only provide a crude simplification of the full anatomical information. Instead, we propose a measure of brain asymmetry that is based on spectral shape descriptors from the *BrainPrint* (Wachinger *et al.*, 2015). Shape vectors are more sensitive to anatomical variations and consequently have the potential to detect finer localized variations, e.g. early morphological changes in subnuclei. Different effects of Alzheimer's disease on the anterior versus the posterior hippocampus have, for instance, been reported in Woolard and Heckers (2012), supporting the assumption of increasing shape asymmetry without any substantial volumetric differences. Furthermore, recent analyses on high-field MRI suggest focal insults in the hippocampal region caused by ageing and dementia, where the subfields subiculum and CA1 are associated with Alzheimer's disease and the subfields CA3 and dentate gyrus are associated with ageing (Pievani *et al.*, 2011; Jagust, 2013). While the subfield segmentation is challenging due to small intensity differences between subfields, low resolution of *in vivo* MRI and partial volume effects, neuroanatomical shape analysis is potentially sensitive to such heterogeneous changes.

Next to retaining more geometrical information, the proposed asymmetry measure offers several advantages: (i) it completely avoids lateral processing bias as it works on both hemispheres independently; (ii) it does not require prior spatial alignment; (iii) it is not restricted to a specific anatomical structure, supporting a brain-wide analysis; and (iv) it presents a within-subject measure that identifies directional and undirectional asymmetry. Directional asymmetry refers to hemispheric differences that show a stronger effect on one of the hemispheres, e.g. higher changes on the left than on the right. Undirectional asymmetry does not have a consistent hemispheric effect and therefore refers to the magnitude of asymmetry independent of direction. Our results suggest a strong increase in shape asymmetry with the progression of dementia that is undirectional. Alternative approaches, such as voxel-wise techniques or statistical shape models compute statistics across the population and are well suited for measuring directional asymmetry, but they cannot detect undirectional asymmetry. We believe that the sensitive representation of geometry together with ability to identify undirectional asymmetry are key aspects for revealing increased asymmetries with the progression of dementia.

Longitudinal trajectories during cognitive decline

To derive disease trajectories of brain asymmetry, individuals should be ideally followed for the full time period of

interest. This, however, creates numerous practical problems related to technology, funding, and logistics (Thompson *et al.*, 2011). One possible alternative is to use cross-sectional designs, but they can confound within- and between-individual variation (Schaie and Caskie, 2005). This is especially problematic for neurodegenerative diseases where premature dropout may be caused by advanced disease progression. The unstructured multi-cohort longitudinal design in the Alzheimer's Disease Neuroimaging Initiative (ADNI) presents an attractive alternative. On the one hand, it covers a wide age range by collecting data from multiple age cohorts. On the other hand, it can identify within-subject effects by following individuals longitudinally for a certain time period, which is typically only a fraction of the total age range of the study (Thompson *et al.*, 2011). Here we use mixed effects models (Verbeke and Molenberghs, 2009; Thompson *et al.*, 2011; Fitzmaurice *et al.*, 2012; Bernal *et al.*, 2013) to differentiate across- and within-individual variations in brain asymmetry.

Survival analysis for predicting progression to Alzheimer's disease

In addition to the analysis of disease trajectories, we investigate whether brain asymmetry is significantly associated with the progression of MCI patients to Alzheimer's disease. This helps in understanding the nature of neurobiological changes at a critical phase in the disease and in assessing the response to treatment. Formulating the differentiation between progressors and non-progressors as group comparison is one possibility (Chetelat *et al.*, 2005; Jack *et al.*, 2008*a*; Cuingnet *et al.*, 2011), but it requires the selection of an arbitrary time frame of progression (e.g. 18 or 36 months) and it does not account for censoring or drop-out of individuals. Survival analysis (also time-to-event analysis) presents an appropriate statistical treatment of the progression to Alzheimer's disease by explicitly modelling the timing of the event and by considering the finite follow-up time. Most prior studies in neuroimaging that apply time-to-event analysis work with time-independent explanatory variables (Devanand *et al.*, 2007; Marcus *et al.*, 2007; Geerlings *et al.*, 2008; Desikan *et al.*, 2009, 2010; Vemuri *et al.*, 2011; Da *et al.*, 2014). Such models only use the information from a single baseline scan and do not integrate the information from follow-up assessments in longitudinal studies, thus ignoring valuable data. A recent approach proposes the application of survival analysis with time-dependent variables (Sabuncu *et al.*, 2014) to investigate hippocampal volume and cortical thickness in a mass-univariate analysis. In contrast, here we use time-varying shape asymmetry measures derived from the *BrainPrint* for studying progression to Alzheimer's disease. We overcome the challenge of integrating time-dependent variables that require observations at all event time points by using the previously mentioned mixed effects models for inference.

Materials and methods

Overview

Figure 1 presents a graphical overview of the computation of brain asymmetry with the *BrainPrint*, which is an ensemble of shape descriptors that are computed on cortical and subcortical structures. The Mahalanobis distance between lateralized shapes yields the measure of shape asymmetry. Due to the holistic representation of brain morphology in the *BrainPrint*, we compute shape asymmetries on 11 lateralized brain structures, which is in contrast to previous studies on shape analysis in Alzheimer's disease that typically focused on the hippocampus (Ferrarini *et al.*, 2009; Gerardin *et al.*, 2009; Costafreda *et al.*, 2011; Lindberg *et al.*, 2012; Shen *et al.*, 2012). The extensive characterization of neuroanatomy is a promising avenue for diagnosing Alzheimer's disease, considering that it is associated with global atrophy across the entire brain (Fjell *et al.*, 2013). Recent results for the prediction of dementia at an international challenge (Bron *et al.*, 2015) indicate the potential of *BrainPrint* for studying Alzheimer's disease (Wachinger *et al.*, 2014; Wachinger and Reuter, 2016). *BrainPrint* naturally extends the contemporary region of interest-based volume and thickness analysis with shape information. The significance of a descriptive representations of the data is highlighted by results in pattern recognition suggesting that it is less the classifier but rather the representation that primarily impacts the performance of a predictive model (Dickinson, 2009).

The brain descriptor BrainPrint

The *BrainPrint* (Wachinger *et al.*, 2015) description is based on the automated segmentation of anatomical brain structures with FreeSurfer (Dale and Sereno, 1993; Dale *et al.*, 1999; Fischl *et al.*, 1999*a*, *b*, 2002). Images are processed with the longitudinal framework in FreeSurfer (Reuter *et al.*, 2012), which increases intraindividual measurement reliability while avoiding potential processing bias (Reuter and Fischl, 2011). After image segmentation, geometric representations (surface and volumetric meshes) are extracted for the identified cortical and subcortical structures via the marching cubes algorithm. *shapeDNA* (Reuter *et al.*, 2006) is used as the shape descriptor of the individual structures, which performed among the best in a comparison of methods for non-rigid 3D shape retrieval (Lian *et al.*, 2012). *shapeDNA* is based on the (normalized) eigenvalues of the Laplace-Beltrami operator and, therefore, isometry invariant (including rigid motion and reflections). Eigenvalues of the Laplace-Beltrami operator Δ can be computed via finite element analysis by solving the Laplacian eigenvalue problem (Helmholtz equation) on the given shape:

$$\Delta f = -\lambda f \tag{1}$$

The solution consists of eigenvalue $\lambda_i \in \mathbb{R}$ and eigenfunction f_i pairs, sorted by eigenvalues, $0 \leq \lambda_1 \leq \lambda_2 \leq \ldots$ (a positive diverging sequence). The first l non-zero eigenvalues are computed using the finite element methods and form the *shape DNA*: $\overline{\lambda} = (\lambda_1, \ldots, \lambda_l)$, where we set $l = 50$ in this study. To achieve scale independence, we normalize the eigenvalues:

$$\lambda' = \mathrm{vol}^{\frac{2}{D}}\lambda, \tag{2}$$

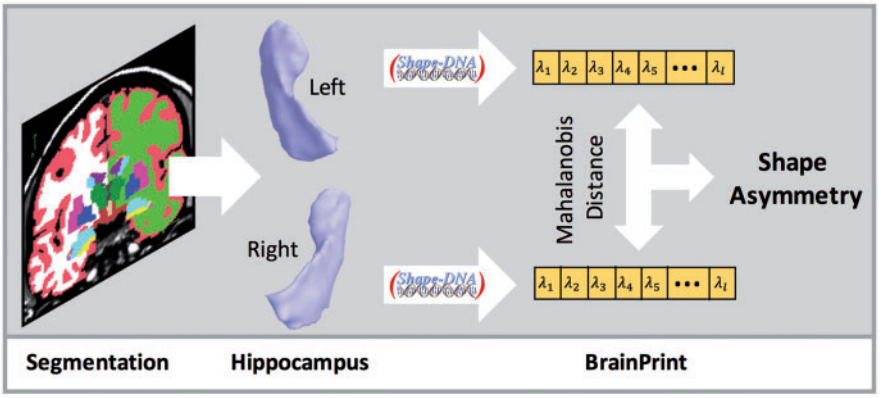

Figure 1 Overview of the computation of shape asymmetry with *BrainPrint*. Based on the brain segmentation, we create meshes from lateralized structures, e.g. the hippocampus. The computation of the shape descriptor *shapeDNA* yields the characteristic spectrum of the shape, λ, that form the *BrainPrint*. The Mahalanobis distance between the spectra of both hemispheres results in the shape asymmetry.

where vol is the Riemannian volume of the D-dimensional manifold (Reuter *et al.*, 2006), i.e. the surface area for 2D manifolds, or the volume for 3D solids.

A key property of the eigenvalues is their isometry invariance, i.e. length-preserving deformations will not change the spectrum. Isometry invariance includes rigid body motion as well as reflections and, therefore, permits the comparison of shapes across individuals or hemispheres by directly comparing the *shapeDNA* without any complex and potentially error-prone image or geometry registration. A second property is that the spectrum continuously changes with topology-preserving deformations of the boundary of the object. These properties make the *shapeDNA* well suited for comparing shapes, as initial alignment of the shapes can be completely avoided and similar shapes will have a similar spectrum. We compute the spectra for all subcortical structures on the 2D boundary surfaces (triangle meshes) and for cortical structures on the full 3D solid (tetrahedra meshes created from white and pial surfaces), forming the *BrainPrint* $\Lambda = (\overline{\lambda}_1, \ldots, \overline{\lambda}_\eta)$ (Wachinger *et al.*, 2015).

Figure 2 illustrates the first six non-constant eigenfunctions of the hippocampus. The eigenfunctions show natural vibrations of the shape when oscillating at a frequency specified by the square root of the eigenvalue. For localizing shape changes of the hippocampus, we use the level set analysis for the first eigenfunction as proposed for the caudate in Reuter *et al.* (2009). Figure 2 illustrates level sets as green curves. We compute the circumference of 100 level sets and average among 10 to increase robustness to noise, yielding 10 length measurements per hippocampus. The first eigenfunction presents a natural parameterization of the hippocampus, which we use to localize asymmetry by computing the difference of circumferences across hemispheres and by computing statistics across the population.

Brain asymmetry from BrainPrint

Based on the *BrainPrint*, we measure the asymmetry of lateralized brain structures. As *shapeDNA* is invariant to reflections, we can directly compute the Mahalanobis distance between the descriptors of a lateralized brain structure s

$$Y_s = \| \overline{\lambda}_s^{\text{left}} - \overline{\lambda}_s^{\text{right}} \|_{\Sigma_s}, \quad (3)$$

with Σ_s the covariance matrix across all individuals for structure s (Wachinger *et al.*, 2015). The Mahalanobis distance accounts for the covariance pattern in the data and supports an equal contribution of all eigenvalues in the sequence. This approach completely avoids lateral processing bias as it works on both hemispheres independently. Due to the pose invariance of spectral shape descriptors we can directly measure shape asymmetry by computing the distance in a symmetric fashion—a task that can be rather involved for most other shape representations that first require the construction of local correspondences. In fact, choosing a target hemisphere for registration can potentially bias subsequent analyses. When both hemispheres are not treated exactly the same, e.g. one hemisphere remains untouched while the other gets aligned and resampled, resulting interpolation artefacts can easily cause spurious effects (Reuter and Fischl, 2011; Reuter *et al.*, 2012).

The asymmetry measure presents a within-subject measure that can identify directional and undirectional asymmetry. The difference of eigenvalues can be used to differentiate directional and undirectional asymmetry. We compute the asymmetry for 11 lateralized structures: cerebral white matter, pial region, cerebellum white/grey matter, lateral ventricles, hippocampus, amygdala, thalamus, caudate, putamen, and accumbens. For white matter and pial region, the analysis is performed on volumetric meshes.

Mixed effects models

We used linear mixed effects models (Verbeke and Molenberghs, 2009; Thompson *et al.*, 2011; Fitzmaurice *et al.*, 2012; Bernal *et al.*, 2013) to study cross-sectional and longitudinal effects of brain asymmetry. We denote the age at baseline for individual i with B_i, the years-from-baseline at follow-up scan j with X_{ij}, and the diagnosis with D_i. The linear model for the lateral shape distance Y_{ij} as dependent variable is

$$Y_{ij} = \beta_0 + \beta_1 B_i + \beta_2 X_{ij} + \beta_3 D_i + b_{0i} + b_{1i} X_{ij}, \quad (4)$$

where $\beta_0, \beta_1, \beta_2, \beta_3$ are fixed effects regression coefficients and b_{0i}, b_{1i} are random effects regression coefficients. The random effects enable modelling individual-specific intercept and slope

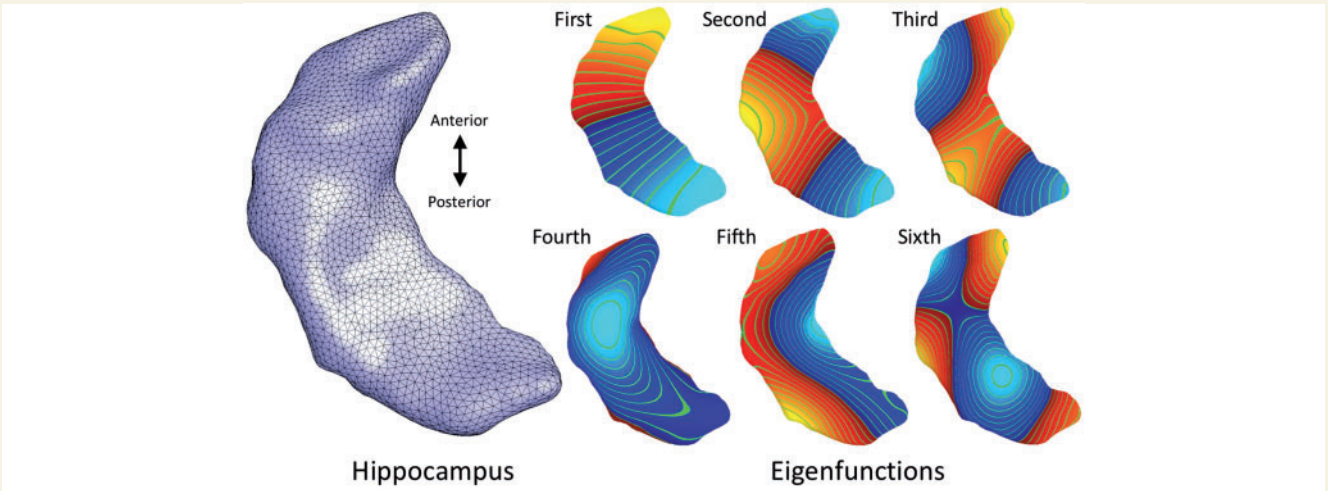

Figure 2 Hippocampus mesh and first six non-constant eigenfunctions of the Laplace-Beltrami operator calculated on the surface. Sorted *left* to *right*, *top* to *bottom*. Increasing positive values of the eigenfunctions are shown in the colour gradient from red to yellow and decreasing negative values are shown from dark blue to light blue. Level sets are shown in green.

with respect to the time from the baseline. We also consider an extended model with the addition of the interaction between diagnosis and years-from-baseline ($X_{ij} \cdot D_i$) to Equation 4, allowing the longitudinal slopes to vary across the different disease groups. Furthermore, we evaluated the interactions between diagnosis and cognitive decline as well as diagnosis and age, but they were not significant. Similarly, a quadratic age term was not significant and a quadratic term for years-from-baseline in the random effect was rejected based on model comparison with AIC (Akaike information criterion) and BIC (Bayesian information criterion). The following additional parameters are included as fixed effects (not shown in Equation 4): years of education, sex, intracranial volume (ICV), and presence of an *APOE4* risk allele. The linear mixed effects model is also used for the statistical analysis of the level sets, where the dependent variable is the absolute difference of the circumferences of level sets between left and right hippocampus.

To analyse regional association of cortical atrophy with increasing hippocampal asymmetry we use a linear model for cortical thickness T_{ij}

$$T_{ij} = \beta_0 + \beta_1 Y_{ij} + \beta_2 B_i + b_{0i}, \quad (5)$$

where $\beta_0, \beta_1, \beta_2$ are fixed effects regression coefficients for intercept, time-varying hippocampal asymmetry Y_{ij} and baseline age B_i of subject i. Again the fixed effects of sex, years of education and presence of APOE4 risk allele are included (not shown in the equation). b_{0i} are random effects regression coefficients for subject-specific offsets. The mass-univariate analysis on the cortex is performed as described in Bernal-Rusiel *et al.* (2013). *P*-values are false discovery rate (FDR) thresholded by $q = 0.05$ (Benjamini and Hochberg, 2000).

Cox proportional hazards model

We use the Cox proportional hazards model (Cox, 1972) for analysing the progression to Alzheimer's disease. Cox regression is a semi-parametric model; the baseline hazard function is not specified and can therefore vary for each unique event time adding flexibility. The hazard function $h(t)$ represents the instantaneous potential for an event at time t, given that no event occurred up to time t. The classical Cox model assumes time-independent explanatory variables and, therefore, only relies on information from baseline scans. For integrating longitudinal data in the analysis, we consider an extended Cox model that combines time-independent variables X and time-dependent variables $Y(t)$

$$h(t, X, Y(t)) = h_0(t) \cdot \exp\left(\sum_{i=1}^{p} \gamma_i X_i + \sum_{j=1}^{q} \delta_j Y_j(t)\right), \quad (6)$$

where $\gamma_1, \ldots, \gamma_p$ are coefficients of the time-independent variables and $\delta_1, \ldots, \delta_q$ are coefficients of the time-dependent variables. The baseline hazard function $h_0(t)$ is not explicitly modelled in Cox, which requires partial likelihood maximization for inferring the model coefficients. In contrast, parametric hazard regression models can employ the more efficient maximum-likelihood estimates but involve making potentially arbitrary assumptions about the baseline hazard. With the Cox model, we account for left truncation and right censoring of the data.

As noted by Sabuncu *et al.* (2014), the fundamental challenge for using longitudinal data in a Cox regression model with time-dependent variables is the necessity to observe all time-dependent variables at each event time. Event times are all time points where events occur across the entire population. Consequently, we require observations for an individual at all event times until he or she experiences the event or is censored. However, scans are not available for all event times in typical longitudinal neuroimaging studies. We therefore need to estimate the imaging markers at times of the clinical events, for which we use the mixed effects models. The improvement of using mixed effects models for Cox regression in comparison to line fitting is described in Sabuncu *et al.* (2014).

For the Cox proportional hazards model in Equation 6, we include the following time-independent covariates: baseline age, sex, ICV, *APOE* genotype status (true if carrier of e4

risk allele), and education. Time-varying variables are years-from-baseline and lateral asymmetry. Testing the proportional hazards assumption using Schoenfeld's residuals results in a significant violation for *APOE4* ($P < 0.05$). We add the interaction between *APOE4* and years-from-baseline to resolve the violation. This interaction is supported by the assumption that APOE4 accelerates atrophy during the prodromal phases of Alzheimer's disease (Jack *et al.*, 2008*b*) and has also been added in Sabuncu *et al.* (2014).

ADNI data

We use data from the Alzheimer's Disease Neuroimaging Initiative (ADNI, adni.loni.usc.edu), which was launched in 2003 by the National Institute on Aging (NIA), the National Institute of Biomedical Imaging and Bioengineering (NIBIB), the Food and Drug Administration (FDA), private pharmaceutical companies and non-profit organizations, as a $60 million, 5-year public–private partnership. The primary goal of ADNI has been to test whether serial MRI, PET, other biological markers, and clinical and neuropsychological assessment can be combined to measure the progression of MCI and early Alzheimer's disease. Determination of sensitive and specific markers of very early Alzheimer's disease progression is intended to aid researchers and clinicians to develop new treatments and monitor their effectiveness, as well as lessen the time and cost of clinical trials. The principal investigator of this initiative is Michael W. Weiner, MD, VA Medical Center and University of California, San Francisco. ADNI is the result of efforts of many co-investigators from a broad range of academic institutions and private corporations, and individuals have been recruited from over 50 sites across the USA and Canada. The follow-up duration of each group is specified in the protocol for ADNI. For up-to-date information, see www.adni-info.org.

Materials and data availability

shapeDNA and the *BrainPrint* software are available at http://reuter.mit.edu/software/ and https://github.com/reuter-lab/BrainPrint. ADNI data are available at adni.loni.usc.edu.

Results

Within- and across-individual changes in asymmetry

Cases with at least three scans are selected from the ADNI cohort, yielding $n = 697$ individuals with summary statistics listed in Supplementary Table 1.

We use a mixed effects model that includes a global intercept β_0, age at baseline β_1, years-from-baseline β_2 and diagnosis [categorical variable β_3 with four groups: controls, MCI stable (MCI-s), MCI progressor (MCI-p) and Alzheimer's disease (AD)], where both the intercept and years-from-baseline are modelled as random effects. Years of education, sex, ICV, and presence of an *APOE4* risk allele are included as additional fixed control variables. The model is explicitly shown in Equation 4. Table 1 reports standardized regression coefficients and *P*-values for the model. For the diagnosis variable, Table 1 shows changes between adjacent diagnostic groups together with the change from controls to Alzheimer's disease. The asymmetry of brain structures is the dependent variable, with results for volume asymmetry (absolute lateral volume difference) on the top and for shape (*BrainPrint*) asymmetry on the bottom. *P*-values that survive FDR correction (Benjamini and Hochberg, 2000) (at $q = 0.05$) are printed in bold.

Compared to volume asymmetry, shape asymmetry demonstrates a stronger association with age, years from baseline, and diagnosis for most structures. For volume asymmetry, a substantial number of structures is significant for the comparison of controls and Alzheimer's disease yet, almost no structure reaches significance for the more challenging differentiation between adjacent diagnostic groups, with the exception of white matter and pial surfaces for MCI-s → MCI-p.

When working with shapes, white matter, cerebellum cortex, hippocampus, amygdala, thalamus, caudate and putamen show a significant lateral shape asymmetry increase with age β_1. For the longitudinal increase of shape asymmetry with years-from-baseline β_2, also the ventricle and accumbens exhibit a significant effect. The longitudinal increase is usually two to five times stronger than the cross-sectional, indicating that asymmetry tends to increase faster as a function of within-individual change in age than as a function of cohort age. The strongest longitudinal effects of shape asymmetry are present in hippocampus, amygdala and putamen.

Shape asymmetries of the hippocampus and amygdala differ significantly across all diagnostic groups. Other structures with significant effects across adjacent diagnostic groups are white matter, pial, and caudate. Especially when comparing controls and Alzheimer's disease (CN → AD) shape asymmetries of almost all structures are significantly different, except for ventricle and thalamus. To further evaluate the association between asymmetry and cognitive decline, we replaced the diagnosis in the mixed effects models with outcomes from cognitive tests. Supplementary Table 3 reports results for the Mini-Mental State Examination (MMSE), Clinical Dementia Rating sum of boxes (CDR-SB) together with the Alzheimer's Disease Assessment Scale (ADAS) with 11 and 13 items. A separate model is estimated for each score. Consistent with the previous results, the strongest and most significant effect is present for the hippocampus and amygdala. Also highly significant across all scores are caudate and cerebellum cortex. For all significant structures we see higher asymmetry for advanced cognitive decline.

We visualize the change in asymmetry for hippocampus, amygdala, and caudate in Fig. 3, which displays the estimated intra- and interindividual change of the lateral shape asymmetry. Solid lines depict the global age effect, where the offset is determined by the diagnostic group variable. Short line ticks depict the longitudinal intraindividual effect which, except for Fig. 3B, is fixed across age and group.

Table 1 Standardized regression coefficients and *P*-values (in parentheses, bold values survive FDR correction at $q = 0.05$) for the analysis of lateral asymmetry with the linear mixed effects model

	β_1	β_2	β_3 (Diagnosis)			
Structure	**(Age)**	**(Years-from-BI)**	**CN → MCI-s**	**MCI-s → MCI-p**	**MCI-p → AD**	**CN → AD**
Volume asymmetry						
White matter	0.010 (0.039)	**0.054 (0.000)**	0.20 (0.010)	**0.27 (0.002)**	0.17 (0.085)	**0.64 (0.000)**
Pial	0.003 (0.448)	0.022 (0.167)	0.18 (0.011)	**0.28 (0.000)**	0.03 (0.707)	**0.49 (0.000)**
Ventricle	**0.016 (0.002)**	**0.058 (0.000)**	0.09 (0.249)	0.02 (0.807)	−0.07 (0.474)	0.05 (0.627)
Cerebellum white matter	0.007 (0.179)	**0.031 (0.048)**	0.07 (0.376)	0.03 (0.756)	0.03 (0.768)	0.13 (0.166)
Cerebellum cortex	0.001 (0.885)	−0.014 (0.214)	0.04 (0.623)	−0.02 (0.824)	−0.10 (0.355)	-0.08 (0.442)
Hippocampus	0.011 (0.053)	0.013 (0.198)	0.13 (0.165)	0.02 (0.863)	0.09 (0.415)	**0.24 (0.024)**
Amygdala	0.009 (0.110)	−0.004 (0.653)	−0.05 (0.562)	0.07 (0.500)	−0.03 (0.779)	-0.02 (0.888)
Thalamus	0.006 (0.273)	**0.029 (0.071)**	0.09 (0.259)	0.03 (0.737)	0.02 (0.814)	0.15 (0.118)
Caudate	**0.019 (0.000)**	0.017 (0.193)	0.13 (0.126)	0.01 (0.927)	0.22 (0.031)	**0.36 (0.000)**
Putamen	0.012 (0.035)	**0.036 (0.004)**	−0.10 (0.259)	0.12 (0.218)	0.10 (0.340)	0.13 (0.216)
Accumbens	0.004 (0.406)	**−0.032 (0.024)**	−0.01 (0.928)	−0.05 (0.616)	0.04 (0.708)	-0.02 (0.864)
Shape asymmetry						
White matter	**0.021 (0.000)**	**0.043 (0.000)**	0.10 (0.241)	**0.29 (0.004)**	−0.04 (0.725)	**0.35 (0.001)**
Pial	0.004 (0.350)	−0.011 (0.486)	**0.18 (0.012)**	0.18 (0.029)	−0.06 (0.474)	**0.30 (0.000)**
Ventricle	0.007 (0.212)	**−0.026 (0.056)**	−0.01 (0.890)	−0.06 (0.510)	0.08 (0.415)	0.01 (0.920)
Cerebellum white matter	0.006 (0.171)	0.006 (0.726)	0.15 (0.026)	−0.06 (0.440)	0.10 (0.248)	**0.19 (0.017)**
Cerebellum cortex	**0.009 (0.030)**	**0.042 (0.023)**	0.08 (0.237)	0.06 (0.442)	0.10 (0.262)	**0.24 (0.003)**
Hippocampus	**0.029 (0.000)**	**0.060 (0.000)**	**0.19 (0.007)**	**0.31 (0.000)**	**0.25 (0.003)**	**0.75 (0.000)**
Amygdala	**0.024 (0.000)**	**0.065 (0.000)**	**0.21 (0.005)**	**0.31 (0.000)**	**0.35 (0.000)**	**0.87 (0.000)**
Thalamus	**0.015 (0.002)**	**0.034 (0.039)**	−0.14 (0.076)	0.01 (0.882)	0.14 (0.146)	0.01 (0.890)
Caudate	**0.015 (0.001)**	**0.057 (0.001)**	−0.02 (0.837)	**0.21 (0.010)**	0.15 (0.103)	**0.34 (0.000)**
Putamen	**0.021 (0.000)**	**0.057 (0.000)**	0.09 (0.312)	−0.01 (0.907)	0.21 (0.040)	**0.29 (0.003)**
Accumbens	0.003 (0.522)	**0.055 (0.001)**	0.10 (0.193)	0.06 (0.489)	0.03 (0.746)	**0.19 (0.033)**

Results are shown for volume (*top*) and shape/*BrainPrint* (*bottom*) asymmetry of neuroanatomical structures. The diagnostic label β_3 is a categorical variable with four groups: controls (CN), MCI stable (MCI-s), MCI progressor (MCI-p), and Alzheimer's disease (AD). The coefficient β_1 is associated to baseline age and β_2 to years-from-baseline. *P*-values are rounded to three decimal places.

The plots confirm the higher intraindividual increase in asymmetry compared to across the age effect. We further see a separation of disease groups for hippocampus and amygdala, consistent with the significant effected reported in Table 1. The model in Equation 4 (used for Fig. 3A, C and D) assumes a constant slope for the intraindividual change across all disease groups. The extended model contains the interaction between years-from-baseline and diagnosis ($X_{ij} \cdot D_i$), which increases its flexibility and permits estimating different slopes for each disease group. In the extended model, we only detect a significant impact of the interaction for the hippocampus [MCI-c: 0.12 ($P = 0.005$); AD: 0.12 ($P = 0.020$)], with the corresponding model plotted in Fig. 3B. Note, that the intraindividual increase for MCI progressor and Alzheimer's disease is similar and much steeper than for MCI stable. The control group shows almost no intraindividual increase in asymmetry, only with respect to age. The interaction between age and disease (different slopes of the permanent lines) was not significant.

The Mahalanobis distance measures the magnitude in shape asymmetry, but does not indicate the direction. To investigate whether the asymmetry is directional, we evaluated the linear mixed effects model for eigenvalue differences across hemispheres of the hippocampus and the amygdala. Table 2 reports the model coefficients for the eigenvalue difference and absolute eigenvalue difference. Results are shown for six eigenvalues of the hippocampus, corresponding to the six eigenfunctions shown in Fig. 2, and for three eigenvalues of the amygdala. The results indicate that there are significantly higher associations for the absolute differences than for the differences, indicating that the pattern of asymmetry is not directional. This is consistent with our results on volume asymmetry, where also the absolute volume difference showed stronger associations than the volume difference. For the interpretation of the eigenvalues, it is instructive to consider the eigenfunctions in Fig. 2, which capture different shape characteristics of the hippocampus, such as length, curvature, thickness, and width.

To localize the part of the hippocampus asymmetry that shows the strongest association with Alzheimer's disease, we use the level-set analysis. We compute the mixed effects model on the absolute difference of level set lengths across hemispheres. Figure 2 illustrates the level sets as green curves of the first eigenfunction. Supplementary Fig. 1 visualizes the *P*-values for comparing controls and Alzheimer's disease (CN → AD). The

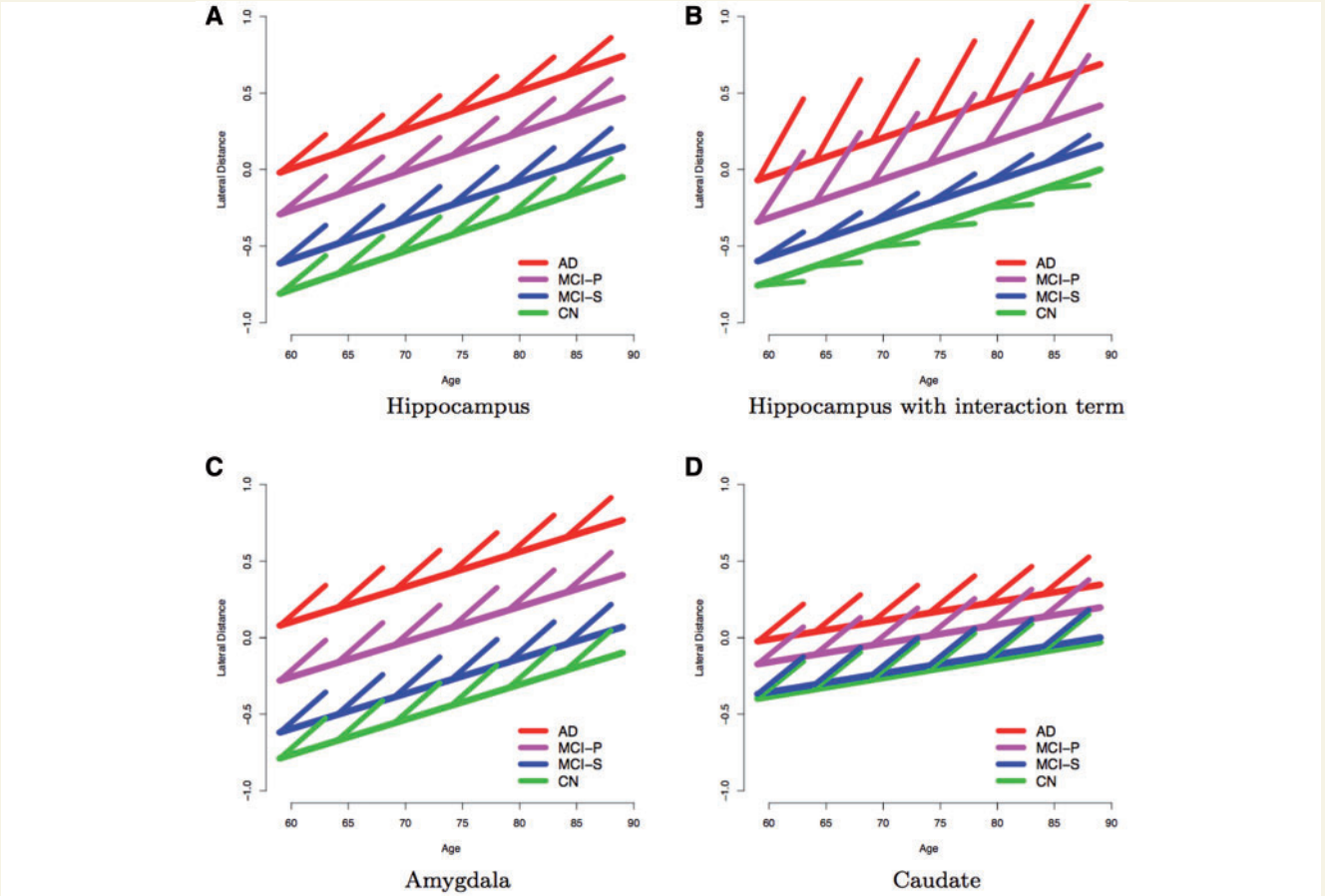

Figure 3 Longitudinal analysis of standardized lateral asymmetry measures of the hippocampus (A and B), amygdala (C), and caudate (D). Lines and ticks illustrate estimates of the different linear mixed effects models. The global age effect (fixed across groups) is depicted by the slope of the long solid lines, the group effect is the offset showing increased asymmetry with advanced disease stage. Short line ticks depict longitudinal slopes. They are parallel across time and group (in **A**, **C** and **D**) and can vary across group (in **B**), depicting the model for the hippocampus with an additional (significant) interaction term between years-from-baseline and diagnosis, showing increasing asymmetry slopes across groups concordant with disease stage. Diagnostic groups are shown in colour and the order of the lines follows the order of the legend from *top* to *bottom*. AD = Alzheimer's disease; MCI-P = MCI progressor; MCI-S = MCI stable; CN = controls.

posterior region is not significantly associated with diagnosis, while the anterior region shows the strongest association ($P < 10^{-5}$).

To further investigate connections between increasing asymmetry and cortical thickness changes, we estimate a slightly different mixed effects model (Equation 5) on the cortex for the mass-univariate analysis of thickness as the dependent variable employing all available subjects and time points. Here, we include a global intercept β_0 and the time-varying hippocampal asymmetry measure β_1. Further, baseline age, sex, years of education, and presence of an *APOE4* risk allele are again included as additional fixed control variables. The intercept is modelled as a random effect. Figure 4 shows the significance map for the longitudinal effect β_1 of hippocampal asymmetry after FDR thresholding, highlighting cortical regions where grey matter atrophy is significantly associated with within-subject increases in hippocampal asymmetry, when controlling for age, sex, education, and *APOE4* status.

Progression from mild cognitive impairment to Alzheimer's disease

For studying the progression from MCI to Alzheimer's disease, we used $n = 374$ individuals with MCI, with diagnostic and demographic information reported in Supplementary Table 2.

For the Cox proportional hazards model with time-varying variables in Equation 3, we evaluate the lateral asymmetry for each of the 11 brain structures with respect to shape (*BrainPrint*) and size (volume). In addition, we compute a classical Cox model on baseline measurements of the *BrainPrint*, yielding 33 Cox models in total. Table 3 reports hazard ratios (HR), confidence intervals (CI), and estimates of statistical significance with the Wald test for the asymmetry component in each model. Figure 5 visualizes the significance for subcortical structures with the *BrainPrint*. The only component that exhibits a significant effect for all models is the interaction between *APOE4* and

Table 2 Standardized regression coefficients and *P*-values (in parentheses, bold values survive FDR correction at $q = 0.05$) for the analysis of lateral asymmetry of the hippocampus (*top*) and amygdala (*bottom*) with the linear mixed effects model

	β_1 (Age)	β_2 (Years-from-BI)	β_3 (Diagnosis) CN → MCI-s	MCI-s → MCI-p	MCI-p → AD	CN → AD
Eigenvalue difference for hippocampus						
Eigenvalue 1	0.003 (0.922)	−0.013 (0.218)	−0.141 (0.043)	0.074 (0.346)	−0.088 (0.295)	−0.156 (0.051)
Eigenvalue 2	0.201 (0.050)	0.025 (0.639)	−0.273 (0.305)	0.602 (0.043)	0.025 (0.939)	0.354 (0.246)
Eigenvalue 3	0.128 (0.468)	0.090 (0.334)	−0.387 (0.397)	−0.083 (0.871)	0.388 (0.485)	−0.082 (0.876)
Eigenvalue 4	0.202 (0.279)	0.186 (0.062)	−0.218 (0.651)	0.812 (0.133)	−0.134 (0.819)	0.460 (0.407)
Eigenvalue 5	−0.050 (0.761)	0.208 (0.033)	0.533 (0.208)	0.091 (0.847)	0.631 (0.220)	1.255 (0.010)
Eigenvalue 6	−0.210 (0.240)	0.120 (0.223)	−0.513 (0.268)	0.598 (0.248)	−0.123 (0.826)	−0.038 (0.943)
Absolute eigenvalue difference for hippocampus						
Eigenvalue 1	0.029 (0.106)	−0.003 (0.746)	−0.020 (0.654)	0.058 (0.255)	0.072 (0.194)	**0.110 (0.036)**
Eigenvalue 2	**0.164 (0.018)**	0.091 (0.034)	0.367 (0.040)	**0.483 (0.015)**	**0.759 (0.001)**	**1.609 (0.000)**
Eigenvalue 3	**0.403 (0.000)**	0.134 (0.069)	0.530 (0.064)	0.256 (0.423)	**1.038 (0.003)**	**1.824 (0.000)**
Eigenvalue 4	**0.536 (0.000)**	0.111 (0.114)	0.289 (0.308)	**0.996 (0.002)**	0.341 (0.324)	**1.626 (0.000)**
Eigenvalue 5	**0.487 (0.000)**	0.121 (0.053)	0.051 (0.842)	**1.183 (0.000)**	0.347 (0.266)	**1.581 (0.000)**
Eigenvalue 6	**0.428 (0.000)**	0.115 (0.108)	0.619 (0.034)	**0.934 (0.004)**	0.280 (0.431)	**1.833 (0.000)**
Eigenvalue difference for amygdala						
Eigenvalue 1	−0.000 (0.995)	−0.029 (0.202)	−0.077 (0.651)	0.124 (0.516)	−0.201 (0.328)	−0.154 (0.427)
Eigenvalue 2	0.180 (0.029)	0.030 (0.467)	0.131 (0.538)	−0.083 (0.729)	0.545 (0.035)	0.593 (**0.015**)
Eigenvalue 3	−0.019 (0.798)	0.000 (1.000)	0.206 (0.291)	−0.120 (0.584)	0.214 (0.369)	0.301 (0.184)
Absolute eigenvalue difference for amygdala						
Eigenvalue 1	**0.111 (0.006)**	0.033 (0.110)	0.075 (0.472)	0.176 (0.131)	**0.309 (0.014)**	**0.559 (0.000)**
Eigenvalue 2	**0.104 (0.023)**	0.061 (0.056)	0.235 (0.047)	**0.330 (0.013)**	**0.561 (0.000)**	**1.126 (0.000)**
Eigenvalue 3	0.092 (0.111)	0.071 (0.029)	0.212 (0.154)	0.261 (0.117)	0.152 (0.404)	**0.625 (0.000)**

The model is similar to the one in Table 1 with the dependent variable replaced by the (absolute) difference of the eigenvalues. The diagnostic label β_3 is a categorical variable with four groups: controls (CN), MCI stable (MCI-s), MCI progressor (MCI-p), and Alzheimer's disease (AD). The coefficient β_1 is associated to baseline age and β_2 to years-from-baseline. *P*-values are rounded to three decimal places. The six eigenfunctions of the hippocampus corresponding to the eigenvalues are shown in Fig. 2.

years-from-baseline. In addition to the significance of separate variables in the model, tests of the overall goodness of fit with the Wald test showed significance for all models.

Structures that show significant results for the *BrainPrint* are cortical structures, hippocampus, amygdala, and caudate. For volume asymmetry measurements, none of the structures demonstrate a significant effect in the model. For the model with *BrainPrint* baseline measurements, hippocampus, amygdala, and putamen have *P*-values below 0.05, but they are not significant after FDR correction. All significant structures have a hazard ratio >1, which means that the increase in asymmetry raises the risk for progression to Alzheimer's disease.

Discussion

Here we present the first method for shape-based asymmetry analysis of dementia. Our method does not require registration, and avoids interpolation artefacts and lateral processing bias by treating both hemispheres exactly the same. We, furthermore, analyse a variety of different subcortical and cortical structures.

Previous studies on hippocampal asymmetry based on volumetry and small sample sizes have not found significant increases with dementia (Fox *et al.*, 1996; Barnes *et al.*, 2005; Shi *et al.*, 2009). Here we demonstrate a clear increase in shape asymmetry of the hippocampus and amygdala concurrent with disease progression (Table 1). We report significant differences in asymmetry across all four diagnostic categories (CN, MCI-s, MCI-p, AD) and observe a similar spacing in baseline asymmetry across diagnostic groups, with MCI progressors about halfway between MCI stable and Alzheimer's disease patients (Fig. 3). These results are further supported by the significant association between asymmetry and cognitive test scores (MMSE, CDR-SB, ADAS11, ADAS13) (Supplementary Table 3) and by within-subject associations of hippocampal asymmetry increase with cortical atrophy (Fig. 4), notably in the temporal lobe (both hemispheres) and superior frontal regions (left hemisphere). The detected increase of subcortical asymmetry is consistent with previous findings from PET imaging that demonstrated asymmetric hypometabolism (Grady *et al.*, 1988; Haxby *et al.*, 1990) and an asymmetric distribution of amyloid-β (Frings *et al.*, 2015), as well as cortical asymmetries (Thompson *et al.*, 2007; Long *et al.*, 2013). The lack of significant asymmetry findings from previous volumetric studies suggests a heterogeneous effect of neurodegenerative mechanisms on subcortical structures that causes neuroanatomical

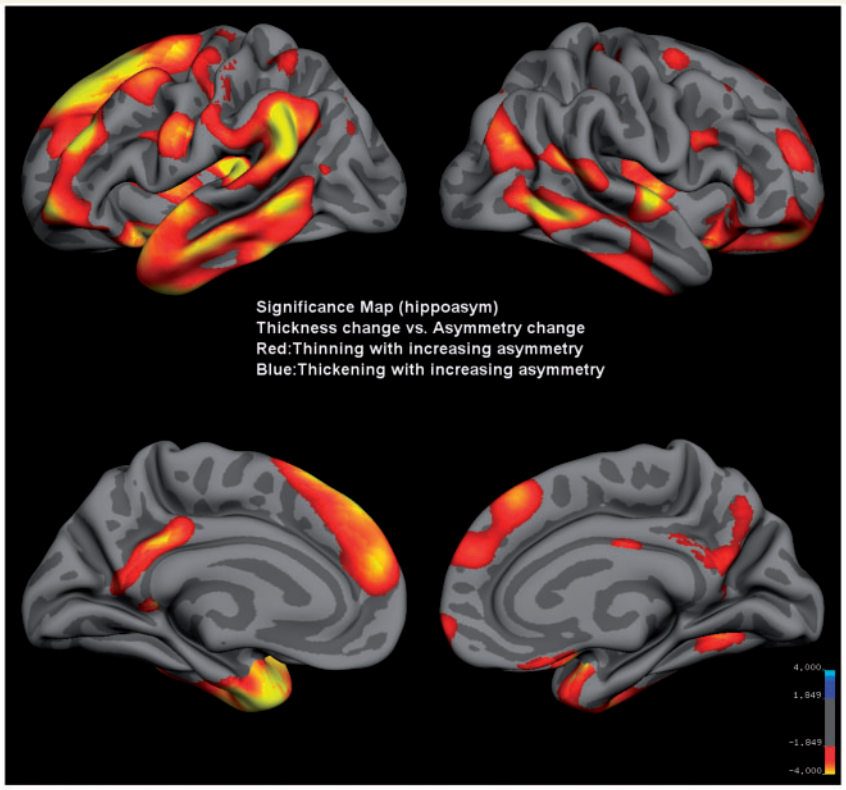

Figure 4 Significance map from a two-sided test. FDR thresholded at $q = 0.05$, yellow: $P \leq 0.0001$. Showing regions where within-subject cortical thickness loss (atrophy) is significantly associated with hippocampal asymmetry increase, controlling for age, sex, education and presence of *APOE4* (unsigned testing).

Table 3 Coefficients from the Cox proportional hazards model for the lateral asymmetry computed with the *BrainPrint* and volume

Structure	*BrainPrint* (time-varying)			Volume (time-varying)			*BrainPrint* (baseline)		
	HR	CI	*P*	HR	CI	*P*	HR	CI	*P*
White matter	1.23	1.03–1.45	**0.019**	1.15	0.98–1.35	0.089	1.10	0.93–1.29	0.268
Pial	1.21	1.03–1.43	**0.024**	1.08	0.91–1.29	0.385	1.08	0.91–1.28	0.388
Ventricle	0.88	0.73–1.08	0.221	1.02	0.84–1.22	0.863	0.87	0.72–1.05	0.156
Cerebellum white matter	1.00	0.82–1.21	0.967	0.95	0.78–1.16	0.616	0.95	0.79–1.14	0.604
Cerebellum cortex	1.05	0.88–1.26	0.569	1.01	0.84–1.21	0.913	0.88	0.73–1.07	0.207
Hippocampus	1.34	1.13–1.58	**0.001**	1.05	0.87–1.25	0.618	1.22	1.03–1.44	0.023
Amygdala	1.30	1.09–1.54	**0.003**	1.04	0.86–1.25	0.717	1.22	1.03–1.44	0.021
Thalamus	0.98	0.81–1.19	0.873	1.10	0.92–1.33	0.295	1.10	0.92–1.32	0.304
Caudate	1.27	1.07–1.52	**0.007**	1.02	0.85–1.23	0.798	1.14	0.98–1.34	0.095
Putamen	1.15	0.96–1.37	0.137	1.17	1.00–1.37	0.053	1.23	1.03–1.47	0.019
Accumbens	1.05	0.87–1.27	0.596	0.95	0.78–1.15	0.572	1.08	0.90–1.30	0.413

For the *BrainPrint*, we evaluated the Cox model with time-varying variables and with baseline measurements, respectively. We report the hazard ratio (HR), the confidence interval (CI), and the *P*-value (*P*) from the Wald test (bold values survive FDR correction at $q = 0.05$).

shape variations. This view is supported by findings that Alzheimer's disease is more prominent in specific subfields of the hippocampus (Pievani *et al.*, 2011; Jagust, 2013) and subnuclei of the amygdala (Mukai *et al.*, 1994). Due to an increase in sensitivity to local shape changes, our shape asymmetry analysis can detect these subtle effects earlier than volumetry.

Our results on the difference of eigenvalues for the hippocampus and amygdala indicate that the increase in asymmetry is undirectional (Table 2). These results are further supported by results of volume asymmetry, where absolute volume differences show a more significant association to diagnosis than plain differences. These results support the notion that there is no dominant direction of hemispheric

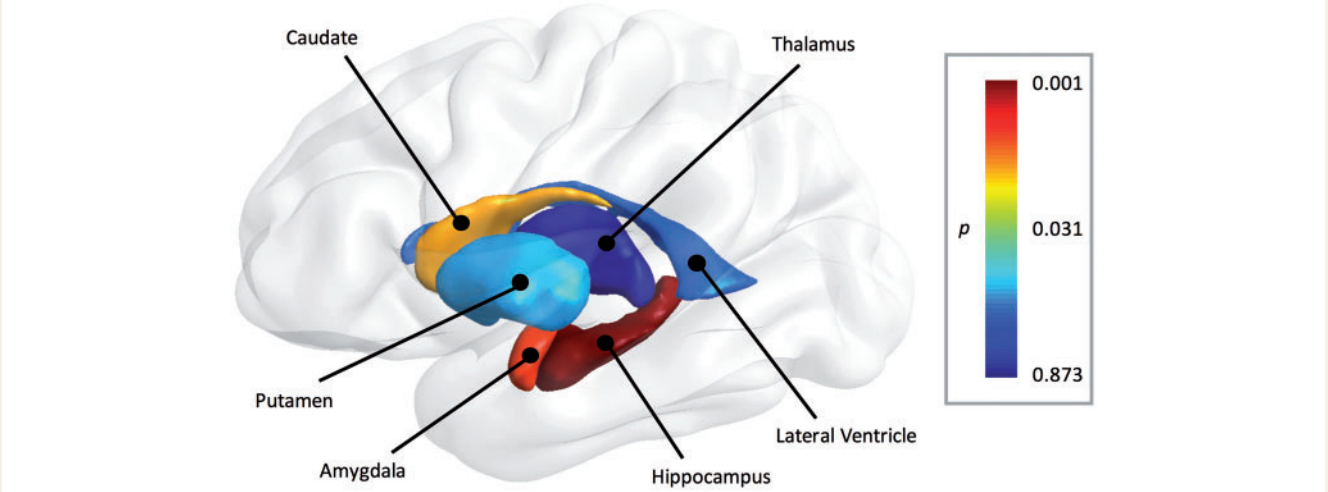

Figure 5 Visualization of the *P*-values of the cox regression model for *BrainPrint* with time-varying variables on subcortical structures.

asymmetry; it is rather the magnitude of the asymmetry that shows significant association with dementia progression. This objects a tentative explanation of higher asymmetry from a possible bias in clinically diagnosing Alzheimer's disease from symptoms potentially more related to left hemisphere atrophy (language-based tests for memory assessment), which could result in directional asymmetry. Alternative approaches, such as voxel-based techniques (VBM, TBM) and statistical shape models, are not well suited for identifying undirectional asymmetry because they average across the population on each hemisphere. In contrast, the proposed shape asymmetry presents a within-subject measure of asymmetry that identifies directional and undirectional asymmetry.

Previous studies on hippocampal asymmetry mainly considered cross-sectional data. Here we find a two to five times higher longitudinal intraindividual increase in asymmetry relative to the cross-sectional age effect (Table 1). These results are in line with previous longitudinal results on cortical thickness (Thompson *et al.*, 2011). Multiple sources of between-patient variation can cause these differences. Most prominent is the healthy survivor effect: individuals with advanced disease progression or low cognitive performance may be more likely to drop-out, thus causing cross-sectional results to be overly optimistic. Sampling variations can further be amplified by non-linear disease trajectories that cause spurious effects in linear models. Evidence for non-linearity is visible in the hippocampus, where the differences in slopes across diagnostic groups is especially pronounced. With the availability of longer follow-up periods and additional time points in the future, the integration of non-linear models may therefore be appropriate. The slope of the MCI progressors is substantially higher than for those that remain stable, as shown by the results of the extended model with the interaction term (Fig. 3B). The longitudinal change of MCI progressors is close to Alzheimer's disease patients, indicating that progressors are on a similar disease trajectory of cognitive decline as Alzheimer's disease patients. The pronounced longitudinal increase in shape asymmetry of progressors allows improved differentiations of progressors from non-progressors when incorporating intraindividual asymmetry changes into the predictive model.

The differentiation between stable MCI and those who progress to Alzheimer's disease is of high clinical relevance, e.g. for selection into disease-modifying therapies or drug trials. Our results from the time-to-event analysis demonstrate that asymmetry is predictive for progression from MCI to Alzheimer's disease for hippocampus, amygdala, caudate and cortex (Table 3 and Fig. 5). Shape asymmetry in these structures may therefore serve as a sensitive biomarker for the progression to Alzheimer's disease. So far, brain asymmetry has not been used for predicting Alzheimer's disease in a time-to-event analysis. A comparison of models with time-varying variables and with baseline measurements shows the advantage of including follow-up measurements in the prediction.

Our results show that shape asymmetry is more predictive of Alzheimer's disease than volume asymmetry. In addition to the results in the mixed effects model, the benefit of shape asymmetry is highlighted in the comparison to volume asymmetry for the progression to Alzheimer's disease in the Cox model, where volumetry did not yield any significant results. This suggests that the coarse representation of a structure by only its volume neglects important information for modelling the onset of dementia. Note, that the asymmetry measure enters all our statistical models as a single scalar value, independent of whether the distance is computed on a high-dimensional shape signature or on the one-dimensional volume. This allows a direct comparison of the *BrainPrint* and the volume-based models and clearly highlights the importance of a discriminative geometric representation for quantifying brain asymmetry. The advantage of shape representations is also underlined

by the level set analysis of the hippocampus, which shows a heterogeneous disease effect across the structure (Supplementary Fig. 1). The anterior hippocampus is primarily implicated by the increase in asymmetry as dementia progresses, consistent with findings from Woolard and Heckers (2012). Such focal effects are likely to be missed by volumetry but high-dimensional shape vectors are sensitive to such localized changes.

Ageing is characterized by a multifaceted set of neurobiological cascades that occur at different rates in different people together with complex and often interdependent effects on cognitive decline (Buckner, 2004). It is therefore not surprising that we detect increasing shape asymmetry in ageing in addition to cognitive decline. The distinction between ageing and dementia-related processes is difficult because regions that accommodate neural systems with high susceptibility to deleterious factors are likely affected by both (Jagust, 2013). While there is a certain overlap, our results also indicate that hippocampus and amygdala show high disease-related effects. In contrast, putamen, thalamus, and white matter show strong ageing associations while being only weakly associated to cognitive decline. Our whole-brain asymmetry analysis, which is in contrast to previous studies that focused on the hippocampus alone, offers new opportunities for disentangling ageing and dementia-related asymmetry increase. The change in asymmetry with age may be a sign of brain plasticity, the adaptation of brain structure throughout life, which is critical for human cognitive evolution (Gómez-Robles *et al.*, 2013). Neuroanatomical asymmetry may be correlated with changes in brain function, which are known to be influenced by a person's life experience. The discriminative analysis of neuroanatomical asymmetry for the whole brain may enable a more detailed analysis of dementia in the future, e.g. the identification of subgroups.

Funding

Support for this research was provided in part by the Humboldt foundation, the National Cancer Institute (1K25CA181632-01), the Massachusetts Alzheimer's Disease Research Center (5P50AG005134), the MGH Neurology Clinical Trials Unit, the Harvard NeuroDiscovery Center, the Genentech Foundation (G-40819), SAP SE, and an NVIDIA hardware award. Further support was provided by the A.A. Martinos Center for Biomedical Imaging (P41RR014075, P41EB015896, U24RR021382), and Shared Instrumentation Grants (1S10RR023401, 1S10RR019307, 1S10RR023043). Data collection and sharing for this project was funded by the Alzheimer's Disease Neuroimaging Initiative (ADNI) (National Institutes of Health Grant U01 AG024904) and DOD ADNI (Department of Defense award number W81XWH-12-2-0012). ADNI is funded by the National Institute on Aging, the National Institute of Biomedical Imaging and Bioengineering, and through generous contributions from the following: Alzheimer's Association; Alzheimer's Drug Discovery Foundation; Araclon Biotech; BioClinica, Inc.; Biogen Idec Inc.; Bristol-Myers Squibb Company; Eisai Inc.; Elan Pharmaceuticals, Inc.; Eli Lilly and Company; EuroImmun; F. Hoffmann-La Roche Ltd and its affiliated company Genentech, Inc.; Fujirebio; GE Healthcare; IXICO Ltd.; Janssen Alzheimer Immunotherapy Research & Development, LLC.; Johnson & Johnson Pharmaceutical Research & Development LLC.; Medpace, Inc.; Merck & Co., Inc.; Meso Scale Diagnostics, LLC.; NeuroRx Research; Neurotrack Technologies; Novartis Pharmaceuticals Corporation; Pfizer Inc.; Piramal Imaging; Servier; Synarc Inc.; and Takeda Pharmaceutical Company. The Canadian Institutes of Health Research is providing funds to support ADNI clinical sites in Canada. Private sector contributions are facilitated by the Foundation for the National Institutes of Health (www.fnih.org). The grantee organization is the Northern California Institute for Research and Education, and the study is coordinated by the Alzheimer's Disease Cooperative Study at the University of California, San Diego. ADNI data are disseminated by the Laboratory for Neuro Imaging at the University of Southern California.

Supplementary material

Supplementary material is available at *Brain* online.

References

Barnes J, Scahill RI, Schott JM, Frost C, Rossor N, Fox NC. Does Alzheimer's disease affect hippocampal asymmetry? Evidence from a cross-sectional and longitudinal volumetric MRI study. Dement Geriatr Cogn Disord 2005; 19: 338–44.

Benjamini Y, Hochberg Y. On the adaptive control of the false discovery rate in multiple testing with independent statistics. J Educ Behav Stat 2000; 25: 60–83.

Bernal JL, Greve DN, Reuter M, Fischl B, Sabuncu MR, Alzheimer's Disease Neuroimaging Initiative. Statistical analysis of longitudinal neuroimage data with linear mixed effects models. Neuroimage 2013; 66: 249–60.

Bernal-Rusiel JL, Reuter M, Greve DN, Fischl B, Sabuncu MR, Alzheimer's Disease Neuroimaging Initiative. Spatiotemporal linear mixed effects modeling for the mass-univariate analysis of longitudinal neuroimage data. Neuroimage 2013; 81: 358–70. doi:10.1016/j.neuroimage.2013.05.049.

Bron EE, Smits M, van der Flier WM, Vrenken H, Barkhof F, Scheltens P, et al. Standardized evaluation of algorithms for computer-aided diagnosis of dementia based on structural MRI: the {CADDementia} challenge. Neuroimage 2015; 111: 562–79.

Buckner RL. Memory and executive function in aging and AD. Neuron 2004; 44: 195–208.

Chetelat G, Landeau B, Eustache F, Mezenge F, Viader F, de La Sayette V, et al. Using voxel-based morphometry to map the structural changes associated with rapid conversion in mci: a longitudinal MRI study. Neuroimage 2005; 27: 934–46.

Costafreda SG, Dinov ID, Tu Z, Shi Y, Liu CY, Kloszewska I, et al. Automated hippocampal shape analysis predicts the onset of dementia in mild cognitive impairment. Neuroimage 2011; 56: 212–19.

Cox DR. Regression models and life-tables. J R Stat Soc Series B Methodol 1972; 34: 187–220.

Cuingnet R, Gerardin E, Tessieras J, Auzias G, Lehéricy S, Habert MO, et al. Automatic classification of patients with Alzheimer's disease from structural MRI: a comparison of ten methods using the ADNI database. Neuroimage 2011; 56: 766–81.

Da X, Toledo JB, Zee J, Wolk DA, Xie SX, Ou Y, et al. Integration and relative value of biomarkers for prediction of MCI to AD progression: spatial patterns of brain atrophy, cognitive scores, APOE genotype and CSF biomarkers. Neuroimage 2014; 4: 164–73.

Dale AM, Fischl B, Sereno MI. Cortical surface-based analysis: I. Segmentation and surface reconstruction. Neuroimage 1999; 9: 179–94.

Dale AM, Sereno MI. Improved localizadon of cortical activity by combining Eeg and Meg with Mri cortical surface reconstruction: a linear approach. J Cogn Neurosci 1993; 5: 162–76.

Desikan RS, Cabral HJ, Fischl B, Guttmann CR, Blacker D, Hyman BT, et al. Temporoparietal MR imaging measures of atrophy in subjects with mild cognitive impairment that predict subsequent diagnosis of Alzheimer disease. Am J Neuroradiol 2009; 30: 532–38.

Desikan RS, Cabral HJ, Settecase F, Hess CP, Dillon WP, Glastonbury CM, et al. Automated MRI measures predict progression to Alzheimer's disease. Neurobiol Aging 2010; 31: 1364–74.

Devanand DP, Pradhaban G, Liu X, Khandji A, De Santi S, Segal S, et al. Hippocampal and entorhinal atrophy in mild cognitive impairment prediction of Alzheimer disease. Neurology 2007; 68: 828–36.

Dickinson SJ. Object categorization: computer and human vision perspectives. Cambridge: Cambridge University Press; 2009.

Ferrarini L, Frisoni GB, Pievani M, Reiber JHC, Ganzola R, Milles J. Morphological hippocampal markers for automated detection of Alzheimer's disease and mild cognitive impairment converters in magnetic resonance images. J Alzheimer Dis 2009; 17: 643–59.

Fischl B, Salat DH, Busa E, Albert M, Dieterich M, Haselgrove C, van der Kouwe A, et al. Whole brain segmentation: automated labeling of neuroanatomical structures in the human brain. Neuron 2002; 33: 341–55.

Fischl B, Sereno MI, Dale AM. Cortical surface-based analysis: II: inflation, flattening, and a surface-based coordinate system. Neuroimage 1999a; 9: 195–207.

Fischl B, Sereno MI, Tootell RBH, Dale AM. High-resolution intersubject averaging and a coordinate system for the cortical surface. Hum Brain Mapp 1999b; 8: 272–84.

Fitzmaurice GM, Laird NM, Ware JM. Applied longitudinal analysis, Vol. 998. Hoboken, NJ: John Wiley Sons; 2012.

Fjell AM, McEvoy L, Holland D, Dale AM, Walhovd KB. Brain changes in older adults at very low risk for Alzheimer's disease. J Neurosci 2013; 33: 8237–42.

Fox NC, Warrington EK, Freeborough PA, Hartikainen P, Kennedy AM, Stevens JM, et al. Presymptomatic hippocampal atrophy in Alzheimer's disease. Brain 1996; 119: 2001–7.

Frings L, Hellwig S, Spehl TS, Bormann T, Buchert R, Vach W, et al. Asymmetries of amyloid-β burden and neuronal dysfunction are positively correlated in Alzheimer's disease. Brain 2015; 138: 3089–99.

Geerlings, MI, den Heijer T, Koudstaal PJ, Hofman A, Breteler MMB. History of Depression, depressive symptoms, and medial temporal lobe atrophy and the risk of Alzheimer sisease. Neurology 2008; 70: 1258–64.

Gerardin E, Chételat G, Chupin M, Cuingnet R, Desgranges B, Kim HS, et al. Multidimensional classification of hippocampal shape features discriminates Alzheimer's disease and mild cognitive impairment from normal aging. Neuroimage 2009; 47: 1476–86.

Gómez-Robles A, Hopkins WD, Sherwood CC. Increased morphological asymmetry, evolvability and plasticity in human brain evolution. Proc R Soc B Biol Sci 2013; 280: 20130575.

Grady CL, Haxby JV, Horwitz B, Sundaram M, Berg G, Schapiro M, et al. Longitudinal study of the early neuropsychological and cerebral metabolic changes in dementia of the Alzheimer type. J Clin Exp Neuropsychol 1988; 10: 576–96.

Haxby, JV, Grady CL, Koss E, Horwitz B, Heston L, Schapiro M, et al. Longitudinal study of cerebral metabolic asymmetries and associated neuropsychological patterns in early dementia of the Alzheimer type. Arch Neurol 1990; 47: 753–60.

Jack CR, Knopman DS, Jagust WJ, Petersen RC, Weiner MW, Aisen PS, et al. Tracking pathophysiological processes in Alzheimer's disease: an updated hypothetical model of dynamic biomarkers. Lancet Neurol 2013; 12: 207–16.

Jack CR, Petersen RC, Grundman M, Jin S, Gamst A, Ward CP, et al. Longitudinal MRI findings from the vitamin E and donepezil treatment study for MCI. Neurobiol Aging 2008a; 29: 1285–95.

Jack CR, Weigand SD, Shiung MM, Przybelski SA, O'Brien PC, Gunter JL, et al. Atrophy rates accelerate in amnestic mild cognitive impairment. Neurology 2008b; 70 (19 Part 2): 1740–52.

Jagust W. Vulnerable neural systems and the borderland of brain aging and neurodegeneration. Neuron 2013; 77: 219–34. doi:http://dx.doi.org/10.1016/j.neuron.2013.01.002.

Lian Z, Godil A, Bustos B, Daoudi M, Hermans J, Kawamura S, et al. A comparison of methods for non-rigid 3D shape retrieval. Pattern Recognit 2012; 46: 449–61.

Lindberg O, Walterfang M, Looi JCL, Malykhin N, Östberg P, Zandbelt B, et al. Hippocampal shape analysis in Alzheimer's disease and frontotemporal lobar degeneration subtypes. J Alzheimer Dis 2012; 30: 355.

Long X, Zhang L, Liao W, Jiang C, Qiu B. Distinct laterality alterations distinguish mild cognitive impairment and Alzheimer's disease from healthy aging: statistical parametric mapping with high resolution MRI. Hum Brain Mapp 2013; 34: 3400–10.

Marcus KJ, Astrakas LG, Zurakowski D, Zarifi MK, Mintzopoulos D, Poussaint TY, et al. Predicting survival of children with CNS tumors using proton magnetic resonance spectroscopic imaging biomarkers. Int J Oncol 2007; 30: 651–57.

Mukai M, Mizutani T, Yamada S. Neuropathological study of the amygdaloid subnuclei in senile dementia of the Alzheimer type, with special reference to the *Basolateral subnuclei*. Neuropathology 1994; 14: 139–47.

Petersen RC, Roberts RO, Knopman DS, Boeve BF, Geda YE, Ivnik RJ, et al. Mild cognitive impairment: ten years later. Arch Neurol 2009; 66: 1447–55.

Pievani M, Galluzzi S, Thompson PM, Rasser PE, Bonetti M, Frisoni GB. APOE4 is associated with greater atrophy of the Hippocampal formation in Alzheimer's disease. Neuroimage 2011; 55: 909–19.

Reuter M, Fischl B. Avoiding asymmetry-induced bias in longitudinal image processing. Neuroimage 2011; 57: 19–21. doi:10.1016/j.neuroimage.2011.02.076.

Reuter M, Schmansky NJ, Rosas HD, Fischl B. Within-subject template estimation for unbiased longitudinal image analysis. Neuroimage 2012; 61: 1402–18. doi:10.1016/j.neuroimage.2012.02.084.

Reuter M, Wolter F-E, Peinecke N. Laplace-beltrami spectra as 'shape-DNA' of surfaces and solids. Comput Aided Des 2006; 38: 342–66. doi:10.1016/j.cad.2005.10.011.

Reuter M, Wolter F-E, Shenton M, Niethammer M. Laplace-Beltrami eigenvalues and topological features of eigen- functions for statistical shape analysis. Comput Aided Des 2009; 41: 739–755.

Sabuncu MR, Bernal-Rusiel JL, Reuter M, Greve DN, Fischl B; Alzheimer's Disease Neuroimaging Initiative. Event time analysis of longitudinal neuroimage data. Neuroimage 2014; 97: 9–18.

Schaie KW, Caskie GIL. Methodological issues in aging research. In Handbook of research methods in developmental science. Hoboken, NJ: John Wiley Sons. 2005, p. 21–39.

Schneider JA, Arvanitakis Z, Leurgans SE, Bennett DA. The neuropathology of probable alzheimer disease and mild cognitive impairment. Ann Neurol 2009; 66: 200–208.

Shen K, Fripp J, Mériaudeau F, Chételat G, Salvado O, Bourgeat P. Detecting global and local hippocampal shape changes in

Alzheimer's disease using statistical shape models. Neuroimage 2012; 59: 2155–66.

Shi F, Liu B, Zhou Y, Yu C, Jiang T. Hippocampal volume and asymmetry in mild cognitive impairment and Alzheimer's disease: meta-analyses of MRI studies. Hippocampus 2009; 19: 1055–64.

Silverman DHS, Small GW, Chang CY, Lu CS, de Aburto MAK, Chen W, et al. Positron emission tomography in evaluation of dementia: regional brain metabolism and long-term outcome. JAMA 2001; 286: 2120–7.

Stefanits H, Budka H, Kovacs GG. Asymmetry of neurodegenerative disease-related pathologies: a cautionary note. Acta Neuropathol 2012; 123: 449–52.

Thompson PM, Hayashi KM, Dutton RA, Chiang M-C, Leow AD, Sowell ER, et al. Tracking Alzheimer's disease. Ann N Y Acad Sci 2007; 1097: 183–214.

Thompson WK, Hallmayer J, O'Hara R. Design considerations for characterizing psychiatric trajectories across the lifespan: application to effects of apoe-e4 on cerebral cortical thickness in Alzheimer's disease. Am J Psychiatry 2011; 168: 894–903.

Vemuri P, Weigand SD, Knopman DS, Kantarci K, Boeve BF, Petersen RC, et al. Time-to-event Voxel-based techniques to assess regional atrophy associated with MCI risk of progression to AD. Neuroimage 2011; 54: 985–91.

Verbeke G, Molenberghs G. Linear mixed models for longitudinal data. Hoboken, NJ: John Wiley & Sons; 2009.

Wachinger C, Batmanghelich K, Golland P, Reuter M. BrainPrint in the computer-aided diagnosis of Alzheimer's disease. In Proceedings MICCAI workshop challenge on computer-aided diagnosis of dementia based on structural MRI data, Boston, MA, USA. 2014.

Wachinger C, Golland P, Kremen W, Fischl B, Reuter M. BrainPrint: a discriminative characterization of brain morphology. Neuroimage 2015; 109: 232–48.

Wachinger C, Reuter M. Domain adaptation for Alzheimer's disease diagnostics. Neuroimage 2016; 139: 470–9. doi: 10.1016/j.neuroimage.2016.05.053

Woolard AA, Heckers S. Anatomical and functional correlates of human hippocampal volume asymmetry. Psychiatry Res 2012; 201: 48–53.